AGU PUBLICATIONS

JGR

Journal of Geophysical Research: Atmospheres

RESEARCH ARTICLE

10.1002/2017JD027212

Special Section:
Fast Physics in Climate Models: Parameterization, Evaluation and Observation

**Key Points:**
- Subgrid orographic drag plays an important roles in the simulation of atmospheric flow
- The drag schemes obviously improve the dynamics over the complex Tibetan Plateau (TP)
- Improvements of TP air temperature and pressure due to subgrid orographic drag are associated with a modified geostrophic balance

**Correspondence to:**
X. Zhou,
xuzhou@itpcas.ac.cn

**Citation:**
Zhou, X., Beljaars, A., Wang, Y., Huang, B., Lin, C., Chen, Y., & Wu, H. (2017). Evaluation of WRF simulations with different selections of subgrid orographic drag over the Tibetan Plateau. *Journal of Geophysical Research: Atmospheres*, *122*, 9759–9772, https://doi.org/10.1002/2017JD027212

Received 27 MAY 2017
Accepted 9 SEP 2017
Accepted article online 27 SEP 2017
Published online 29 SEP 2017



# Evaluation of WRF Simulations With Different Selections of Subgrid Orographic Drag Over the Tibetan Plateau

**X. Zhou[1], A. Beljaars[2], Y. Wang[1,3], B. Huang[4], C. Lin[5], Y. Chen[1], and H. Wu[6]**

[1]Key Laboratory of Tibetan Environment Changes and Land Surface Processes, Institute of Tibetan Plateau Research, Chinese Academy of Sciences, Beijing, China, [2]European Centre for Medium-range Weather Forecasts (ECMWF), Reading, UK, [3]University of Chinese Academy of Sciences, Beijing, China, [4]Department of Energy and Process Engineering, Norwegian University of Science and Technology, Trondheim, Norway, [5]Regional Climate Group, Department of Earth Sciences, University of Gothenburg, Gothenburg, Sweden, [6]State Key Laboratory of Severe Weather, Chinese Academy of Meteorological Sciences, Beijing, China

**Abstract** Weather Research and Forecasting (WRF) simulations with different selections of subgrid orographic drag over the Tibetan Plateau have been evaluated with observation and ERA-Interim reanalysis. Results show that the subgrid orographic drag schemes, especially the turbulent orographic form drag (TOFD) scheme, efficiently reduce the 10 m wind speed bias and RMS error with respect to station measurements. With the combination of gravity wave, flow blocking and TOFD schemes, wind speed is simulated more realistically than with the individual schemes only. Improvements are also seen in the 2 m air temperature and surface pressure. The gravity wave drag, flow blocking drag, and TOFD schemes combined have the smallest station mean bias (−2.05°C in 2 m air temperature and 1.27 hPa in surface pressure) and RMS error (3.59°C in 2 m air temperature and 2.37 hPa in surface pressure). Meanwhile, the TOFD scheme contributes more to the improvements than the gravity wave drag and flow blocking schemes. The improvements are more pronounced at low levels of the atmosphere than at high levels due to the stronger drag enhancement on the low-level flow. The reduced near-surface cold bias and high-pressure bias over the Tibetan Plateau are the result of changes in the low-level wind components associated with the geostrophic balance. The enhanced drag directly leads to weakened westerlies but also enhances the a-geostrophic flow in this case reducing (enhancing) the northerlies (southerlies), which bring more warm air across the Himalaya Mountain ranges from South Asia (bring less cold air from the north) to the interior Tibetan Plateau.

## 1. Introduction

Subgrid orographic drag parameterizations are a crucial aspect of land-atmosphere momentum interaction in numerical weather prediction and climate models. Through their direct control on the wind speed, the horizontal air mass transport and the exchanges of water and energy between land surface and the atmosphere are affected.

Numerous efforts have been made to parameterize different aspects of subgrid-scale orographic drag in numerical models, such as gravity wave drag (GWD; associated with the orographic variance with horizontal scales larger than 3–5 km) (Boer et al., 1984; Choi & Hong, 2015; Hong et al., 2008; Kim & Arakawa, 1995; Kim & Doyle, 2005; Mcfarlane, 1987; Palmer et al., 1986), drag due to low-level flow blocking (FB) (Choi & Hong, 2015; Kim & Doyle, 2005; Lott & Miller, 1997; Scinocca & McFarlane, 2000; Webster et al., 2003), and turbulent-scale orographic form drag (TOFD) (Beljaars et al., 2004; Grant & Mason, 1990; Jimenez & Dudhia, 2012; Wood et al., 2001; Wood & Mason, 1993). These parameterizations have been included into several weather forecast and climate models (e.g., Zadra et al. (2003) in the Canadian Global Environmental Multiscale model, Beljaars et al. (2004) in the European Centre for Medium-Range Weather Forecasts (ECMWF) Integrated Forecasting System (IFS), Rontu (2006) in the High-Resolution Limited Area Model, Jimenez and Dudhia (2012) in the Weather Research and Forecasting (WRF) model, and Choi and Hong (2015) in the Global/Regional Integrated Model System).

The so-called "Drag project," which was initiated by the Working Group for Numerical Experimentation (WGNE) in the World Meteorological Organization, draws more attention to the parameterization of subgrid-scale drag processes, highlights its role in weather and climate simulations, and emphasizes the importance of surface drag over land. Relevant results from this project show that the parameterized subgrid stress is sensitive to horizontal resolution and highly model dependent (Zadra, 2013). WRF is a widely used model for both short-term weather forecasts and long-term simulation; thus, it is interesting to gain both quantitative and qualitative information on the impact of each subgrid orographic drag process, similar to what has been done for other models in the WGNE drag project (http://collaboration.cmc.ec.gc.ca/science/rpn/drag_project/results_cmc.html). In the WRF model, GWD and FB processes are combined and parameterized as an independent process (hereafter GWD/FB scheme) (Choi & Hong, 2015; Hong et al., 2008; Kim & Arakawa, 1995; Kim & Doyle, 2005), which have proved to improve climate simulations (Choi & Hong, 2015; Gregory et al., 1998; Hong et al., 2008; Kim, 1996). To eliminate the positive bias over valleys and negative bias over mountainous grid cells in wind speed, Jimenez and Dudhia (2012) implemented a TOFD scheme (hereafter JD12 scheme) in WRF by introducing an orographic drag term to the momentum conservation equation in the surface layer to parameterize the unresolved orographic stress by the subgrid orographic variance. However, the atmosphere is affected by drag at different heights due to orography with different horizontal scales. This led to the proposal by Wood et al. (2001) and Beljaars et al. (2004) to specify the effect of orographic form drag with an explicit flux profile decaying with height. An insufficient representation of subgrid orography can lead to systematic biases in numerical weather prediction and climate models (Palmer et al., 1986; Wu & Chen, 1985), especially for the complex Tibetan Plateau (TP), where the direct orographic impacts are stronger than over flat regions. Thus, Zhou et al. (2017) incorporated a new TOFD scheme in WRF, which follows an exponential decay of drag with altitude, developed by Beljaars et al. (2004) (hereafter BBW scheme). It is worth mentioning that the JD12 scheme is stability dependent (Lorente-Plazas et al., 2016) while the BBW scheme is not.

The implementation of the GWD/FB scheme by Choi and Hong (2015), and the BBW TOFD scheme by Zhou et al. (2017) in WRF, has provided important information. Their studies respectively show that (1) the GWD/FB scheme considerably improves the simulation of the global winter atmosphere dynamics for different temporal scales of forecast and (2) the BBW TOFD scheme improves the summer atmosphere dynamics over the Tibetan Plateau. Thus, regional evaluations on the Tibetan Plateau (TP; a terrain complex region) in winter time are highly valuable. In the current study, the dynamical impacts of the above mentioned subgrid orographic drag schemes on the atmosphere are highlighted, and regional simulations over the TP are evaluated against observational data and ERA-Interim reanalysis. The main aim of current study is to quantify the model's performance and try to give suggestions on how to select subgrid orographic drag schemes in WRF for TP regional simulations. The structure of this manuscript is as follows: section 2 gives the model setup including introductions to the different subgrid orographic parameterizations used in the current study; section 3 provides the evaluation of wind fields; section 4 presents the evaluation of 2 m air temperature (T2), surface pressure (PSFC), vertical distribution of air temperature, and geopotential height (GPH); Results are discussed in section 5; section 6 provides a summary with concluding remarks and further work.

## 2. Methods, Model Setup, and Data

### 2.1. Methods and Experimental Setup

Because the subgrid orographic drag on the atmosphere is prominent in mountainous regions, the terrain-complex TP is selected as study domain (Figure 1). One subgrid orographic drag parameterization used in the current study with WRF is the GWD/FB scheme which is a combination of a subgrid GWD scheme and a FB scheme. We define the drag from the GWD/FB scheme as GF drag. It is worth noting that the drag from GWD and FB is stability dependent and that the drag accounts for the orography variation larger than 3–5 km. More details about this scheme can be found in Choi and Hong (2015). Another subgrid orographic drag parameterization is the BBW TOFD scheme, which accounts for the turbulent drag caused by small-scale orography (with horizontal scales typically smaller than 5 km). The key formula of this scheme for wind tendency can be expressed as a stress divergence profile. The TOFD is not stability dependent, and this scheme is only applicable for resolutions larger than 5 km. More details can be found in Beljaars et al. (2004).

We conducted evaluations of WRF using four monthly simulation ensembles with different selections of the subgrid orographic processes as shown in Table 1. The first is the CTRL run, in which no subgrid orographic drag is considered. The others are sensitivity runs: CH run, where only the GWD/FB scheme by (Choi & Hong, 2015) is switched on; BBW run, where only the BBW TOFD scheme is switched on; CHBBW run with the GWD/FB, and BBW TOFD schemes switched on. The reason we did not select the JD12 TOFD scheme is that it has minor impact on the vertical distribution of the wind, air temperature, and GPH (not shown). However,

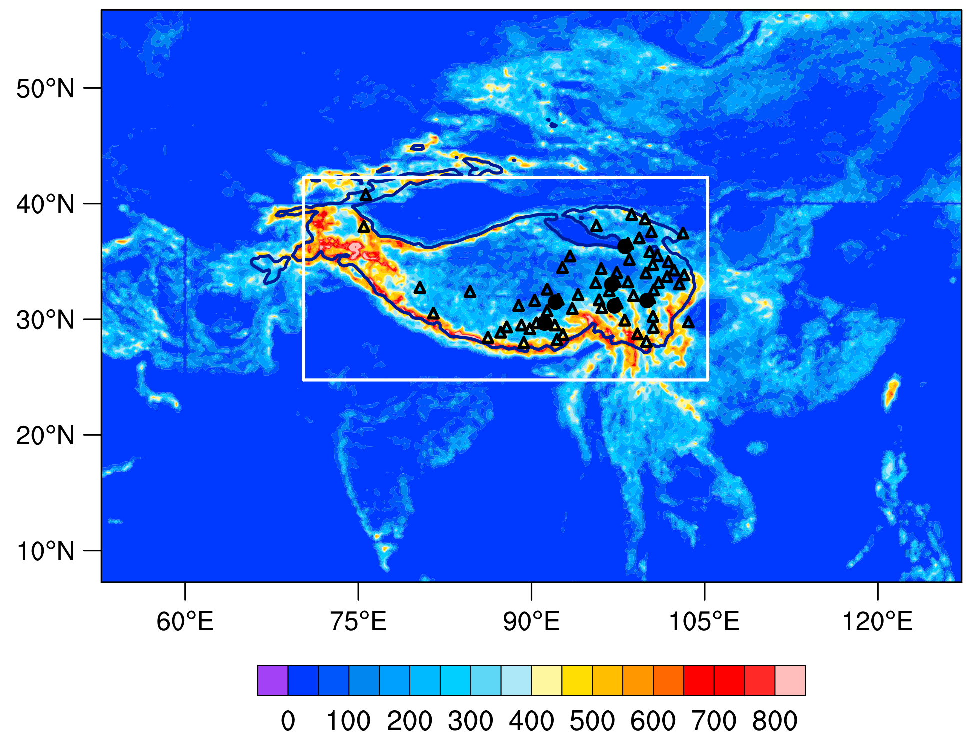


**Figure 1.** The simulation domain; the contour line shows the 3,000 m terrain height; the color indicates the variance (m) of the subgrid orography in 0.25°resolution used in WRF calculated from U.S. Geological Survey (USGS) elevation data; the white line is our focus area, the TP region; the triangles show the CMA station location; and the black points show locations of radio soundings.

one might see benefit in 10 m wind speed in high-resolution simulations using the JD12 scheme (Lorente-Plazas et al., 2016).

The simulation period is December 2007, when, climatologically, precipitation is lowest. The purpose is to conduct a dynamical evaluation without the complexity of the precipitation process. The horizontal resolution is 0.25°. The total number of vertical levels is 37, from the surface to the top of the atmosphere (set to 50 hPa). The model is initialized and driven (for upper and lateral boundaries) by the ERA-Interim reanalysis (Dee et al., 2011) at 6 h intervals. The sea surface temperature is also updated at the same intervals. All the simulations were configured with the Noah land surface model (Chen & Dudhia, 2001), the Yonsei University planetary boundary layer scheme (Hong et al., 2006), and the RRTM scheme (Mlawer et al., 1997) for long-wave and solar radiative transfer.

### 2.2. Data Sets

Three types of data were used for the model evaluation. For comparison, all the simulations have been linearly interpolated to the observation location. The first is daily data at 61 China Meteorological Administration (CMA) weather stations, (available at http://data.cma.cn/data/detail/dataCode/A.0012.0001.html). The CMA station data covers the whole study period without missing values. The second is radio sounding data, which was downloaded from the NOAA Integrated Global Radiosonde Archive (IGRA) website (https://www1.ncdc.noaa.gov/pub/data/igra/). The location of the radio sounding stations is shown in Figure 1. Sounding stations with more than 5 days of missing data are excluded. Daily observations are used for derivation of monthly mean values of the above two data sets. The third one is the ERA-Interim global reanalysis data set from ECMWF based on the IFS model. It has a resolution of approximately 80 km (T255 spectral) on 60 vertical levels from the surface up to 0.1 hPa. ERA-Interim data have also been used to drive the simulations at the domain boundaries.

**Table 1**
*Selection of Subgrid Drag Schemes in Each Simulation*

| Drag schemes case | GWD/FB (Choi & Hong, 2015) | TOFD (Beljaars et al., 2004) |
|---|---|---|
| CTRL run | Off | Off |
| CH run | On | Off |
| BBW run | Off | On |
| CHBBW run | On | On |

## 3. Evaluation of Wind

### 3.1. The 10 m Wind

The main interest is in the TP region due to its high orographic variance (Figure 1). The 10 m wind components (u10 and v10) and absolute wind speed (U10) are compared with CMA station observations. Spatial distribution of the biases in each simulation is shown in Figure 2. Systematic eastward biases of u10 exist in CTRL, eastward biases of u10 occurs in the east of TP of the BBW run, while systematic westward biases of u10 exist in the CH and CHBBW runs. Systematic northward biases of v10 exist in CH and BBW, while the northward biases of v10 in CHBBW only exist in the northeastern part of TP. Systematic overestimations of U10 exist in CTRL, CH, and BBW (east part of interior TP), while the U10 biases in CHBBW are fairly small except for specific stations.

The statistical metrics for each simulation versus station observations are given in Table 2. Introduction of subgrid orographic drag reduces the westerly bias substantially, the RMS error of u10 is reduced by nearly a factor 3, and the correlation coefficient is doubled. However, it is not obvious which of the three configurations (CH, BBW, or CHBBW) is optimal for u10. The v10 bias is larger for CHBBW than CTRL but the RMSE is smaller. CHBBW demonstrates a better simulation of the v10 spatial pattern, which is also proved by the higher $R$ in this run compared to the CTRL run. The RMS error of v10 shows a remarkable reduction, with the best result for CHBBW. The absolute wind speed U10 combines the results of u10 and v10: Introduction of subgrid orographic drag improves bias, RMS error, and $R$ with the best result in all measures for CHBBW.

### 3.2. Vertical Structure of Wind Components

The observed surface wind speed is highly dependent on the precise location of the station within the orographic complexity, while model output only represents the grid mean value. The representativeness of near-surface in situ observations is obviously limited and introduces (mainly random) errors in the verification metrics. Therefore, the surface evaluation is complemented by comparisons of wind profiles with radio sounding observations (six stations as marked in Figure 1 by the black dots) and ERA-Interim for the whole TP region above 3,000 m. There are two reasons that we did not compare the 10 m wind with ERA-Interim data: (1) The terrain height in ERA-Interim is neither the same as observed nor the same as in the WRF simulations. (2) The ERA-Interim surface wind (10 m wind) is only a model forecast and not really analyzed; that is, it is not directly constrained by observations.

Figures 3a1 and 3a2 present the vertical structure of monthly means of station observed, simulated, and ERA-Interim wind components. Figures 3b1, 3b2, 3c1, and 3c2 show the mean biases and RMS errors of simulated and ERA-Interim wind components versus radio soundings. For both $u$ and $v$, ERA-Interim agrees better with observations than the simulations (characterized by a better vertical structure, smaller biases, and RMS errors), which is not a surprise because the soundings were assimilated by ERA-Interim. Nevertheless, ERA-Interim at radio sounding stations still shows some biases. This could come from ERA-Interim model biases (the analysis merges a short range forecast with observations weighted by estimates of forecast and observation errors). Thus, evaluations with both radio sounding stations and ERA-Interim data are necessary. Evaluations with radio sounding can give us a direct quantitative impression of the model's performance, while the validation with ERA-Interim can qualitatively evaluate the model's performance for the whole TP region.

For the study period, the wind from all data sets shows predominantly westerlies that increase from around 0.0 m/s at the surface to a peak of about 55.0 m/s at 200 hPa and then decrease. The magnitude of the meridional wind is typically in the range of ±4 m/s.

The control simulation overestimates systematically the zonal wind throughout the troposphere, and all the drag schemes reduce the bias. The effect of the GWD/FB scheme in CH run is very strong (actually too strong) near the surface and tapers off rather quickly with increasing altitude. The TOFD drag in BBW run is more spread-out in the vertical with a significant reduction of the zonal wind up to 200 hPa. Improvements are also seen in the $v$ component at the low-level atmosphere: the GWD/FB scheme has a strong effect in a shallow layer near the surface where it introduces a northward wind bias. The CH simulation reduces the $v$ errors in the layer from 500 to 400 hPa. The BBW and CHBBW simulations are more modest in the shallow surface layer

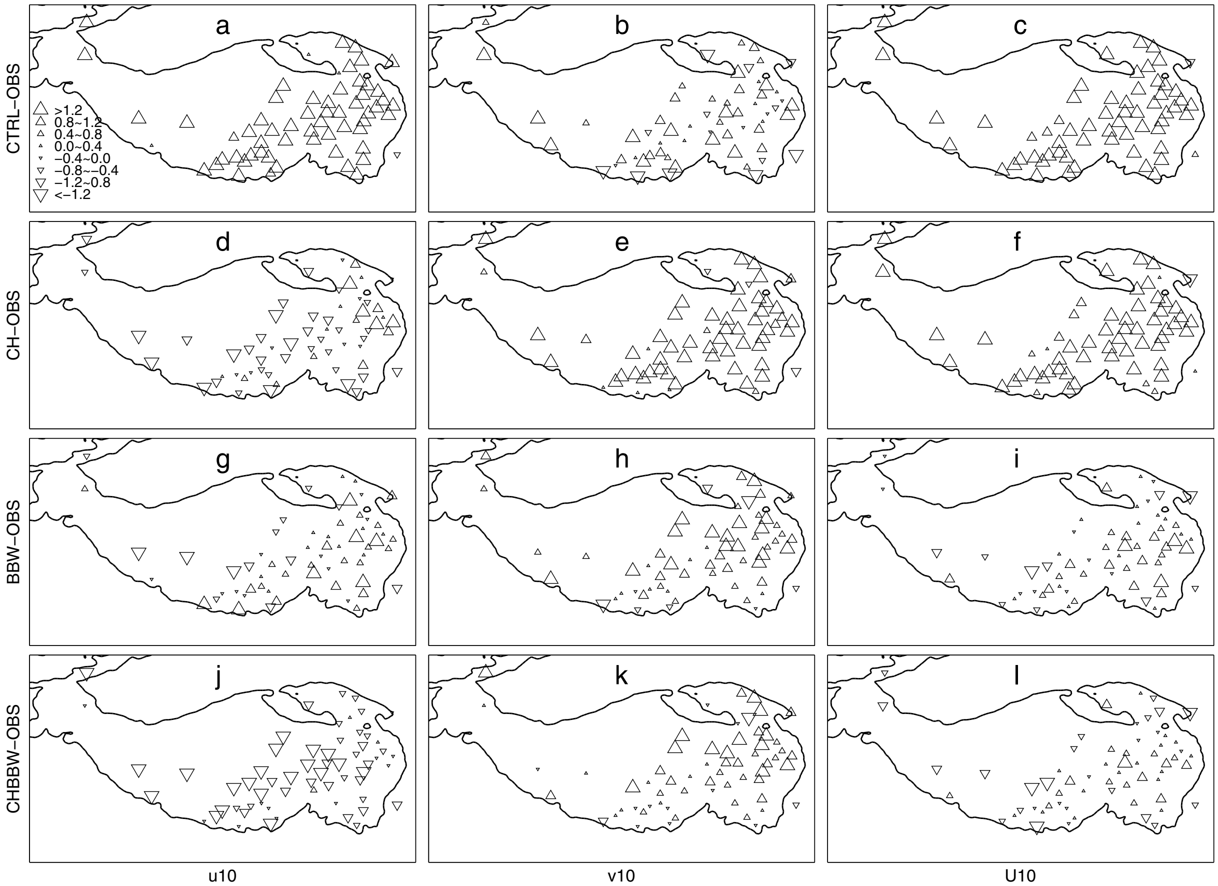


**Figure 2.** Spatial distribution of the monthly mean biases (m/s) in u10, v10, and U10 derived from the (a–c) CTRL run, (d–f) CH run, (g–i) BBW run, and (j–l) CHBBW run minus station observations (OBS).

and improve even further in the 500 to 400 hPa layer. The biases in the *v* component get worse in the upper troposphere with all drag formulations.

The RMS errors mostly confirm the picture seen in the biases. CH reduces the RMS errors in *u* and *v* from the surface up to 300 hPa, whereas BBW and CHBBW improve further. In fact, the RMS error of *u* is improved up to 100 hPa.

ERA-Interim has very good performance compared to the six radio sounding observations. We note that the agreement of ERA-Interim reanalysis data with the radio soundings over TP is also very good in summer (Bao & Zhang, 2013). Also, considering that ERA-Interim drives our experiments at the boundaries, we think that it is reasonable to compare the simulated wind profiles with ERA-Interim as averages over the TP region. The monthly mean wind components, biases, and RMS errors are presented in Figures 3a3, 3a4, 3b3, 3b4, 3c3, and 3c4. Results show that the simulated *u* and *v* components have similar vertical patterns as ERA-Interim. Generally, the BBW and CHBBW runs have smaller *u* and *v* biases than the other two runs, especially

**Table 2**
*Statistical Metrics (Mean Bias; m/s, RMS Error (RMSE; m/s), and Correlation Coefficient R) for the Monthly Mean of u10, v10, and U10 From CTRL Run, CH Run, BBW Run, and CHBBW Run Versus CMA Observations*

| Metrics | u10 | | | v10 | | | U10 | | |
|---|---|---|---|---|---|---|---|---|---|
| case | Bias | RMSE | *R* | Bias | RMSE | *R* | Bias | RMSE | *R* |
| CTRL | 3.24 | 3.26 | 0.33 | 0.49 | 1.33 | 0.30 | 3.24 | 3.57 | 0.11 |
| CH | −0.45 | 0.87 | 0.67 | 1.55 | 1.77 | 0.40 | 2.18 | 2.50 | 0.24 |
| BBW | 0.19 | 0.66 | 0.69 | 0.68 | 1.02 | 0.31 | 0.27 | 0.80 | 0.70 |
| CHBBW | −1.01 | 1.04 | 0.69 | 0.61 | 0.90 | 0.34 | −0.06 | 0.78 | 0.68 |

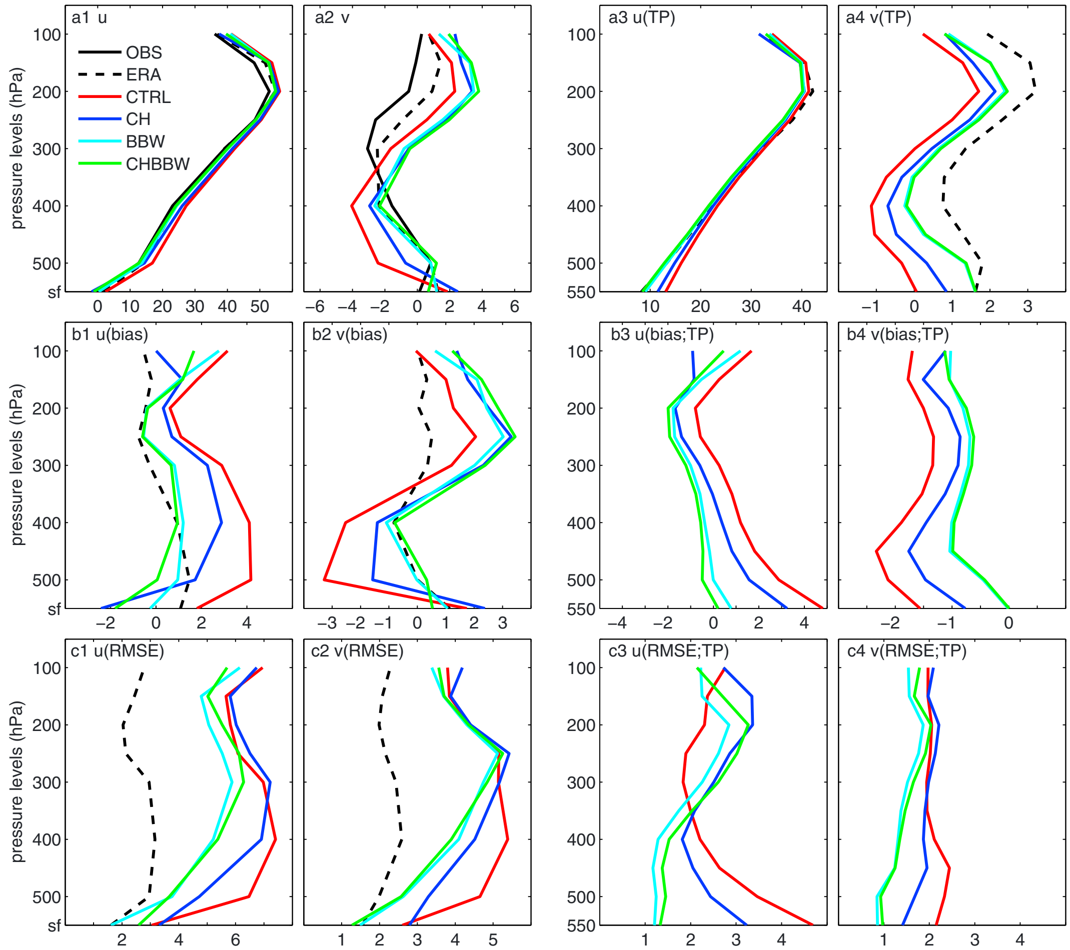


**Figure 3.** Vertical structure of the monthly mean wind components (m/s; a1 and a2 for station mean; a3 and a4 for the whole TP region) derived from radio sounding, ERA-Interim, and four simulations; and the biases (m/s; b1 and b2 for station mean; b3 and b4 for the whole TP region) and RMS errors (m/s; c1 and c2 for station mean; c3 and c4 for the whole TP region) of the wind components derived from CTRL run, CH run, BBW run, and CHBBW run versus radio sounding data (from daily mean), and versus ERA-Interim (from monthly mean).

at lower levels. The CHBBW run also shows a slightly smaller mean $u$ bias than the BBW run, at surface and at 550–350 hPa, but with larger RMS error. It is reassuring that in many respects the comparison with ERA-Interim over the entire TP shows that these subgrid orographic drag schemes improve the simulated low-level flow, similar to what is seen from as the comparison with radio soundings.

## 4. Evaluation of Air Temperature, PSFC, and GPH

### 4.1. T2 and PSFC

The subgrid orographic processes have also indirect impact on the regional and local climate through horizontal air transport and atmosphere-land interactions associated with wind fields. Thus, the simulated T2 and PSFC have been compared with CMA station observations, and the biases are shown in Figures 4a–4h. Before comparison, the simulated T2 and PSFC are corrected with the altitude difference between simulations and station location: T2 is corrected with a general lapse rate of 6°C/km; PSFC is corrected with the equation of static equilibrium ($\Delta p = -\rho g \Delta z$; $\rho$ is the air density, $g = 9.8$ m/s$^2$, and $\Delta z$ is the altitude difference between model and station).

Systematic cold biases and high-pressure biases have been detected for all the simulations. Statistically (Table 3), CTRL has the worst performance with the largest mean bias and RMS error in T2 and PSFC; CH and BBW runs show moderate mean biases and RMS errors; CHBBW has the best performance with smallest mean bias (−2.05°C in T2 and 1.27 hPa in PSFC) and RMS error (3.59°C in T2 and 2.37 hPa in PSFC). The spatial

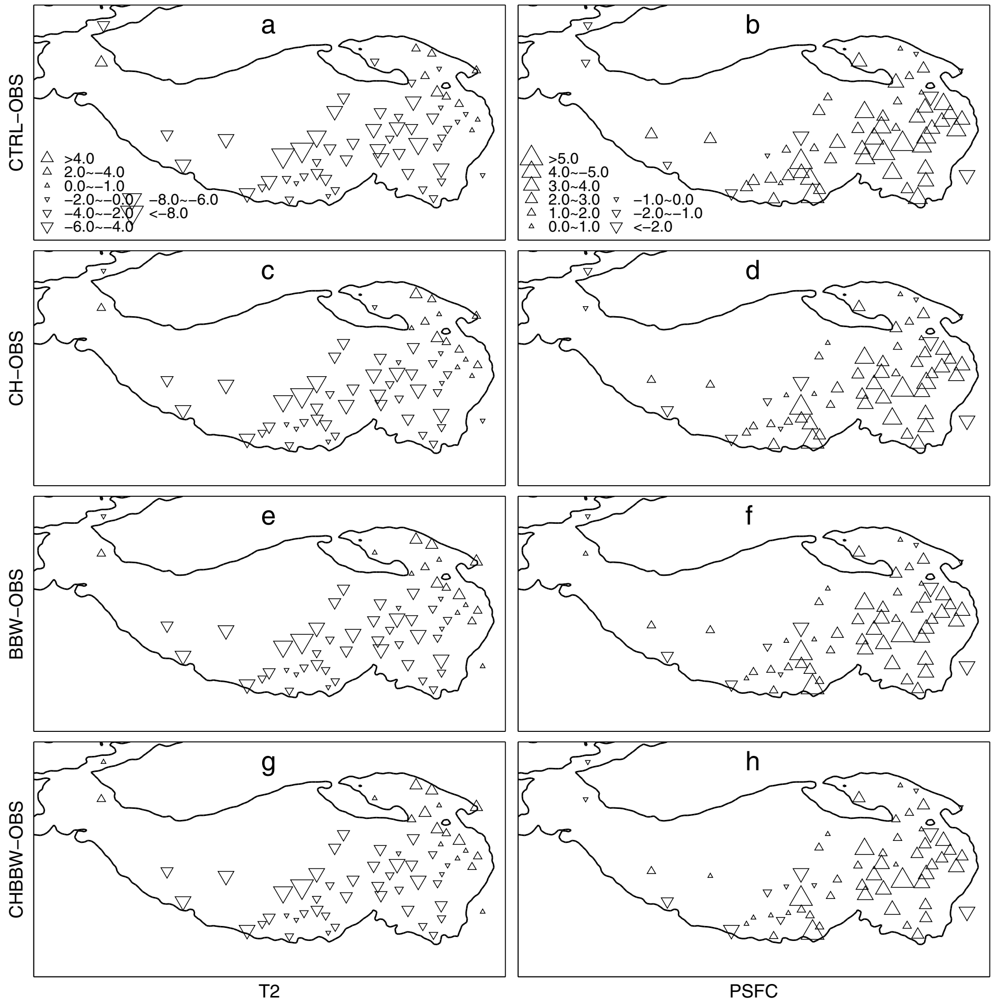


**Figure 4.** Spatial distribution of the monthly mean T2 (°C) and PSFC (hPa) biases derived from the (a and b) CTRL run, (c and d) CH run, (e and f) BBW run, and (g and h) CHBBW run minus station observations (OBS).

*R* is not shown here for these two variables due to the very close values for all the simulations, and they have no help to draw a conclusion. These results demonstrate the indirect improvements by introducing the different subgrid drag components.

Nevertheless, the remaining cold bias, accompanied with the high PSFC bias still exist over the whole TP region. It might be related to local land feedbacks through the surface energy balance, and the associated parameterizations in WRF may need further investigations.

### 4.2. Vertical Structure of Air Temperature and GPH

Figures 5a1 and 5a2 present the vertical structures of monthly mean observed, simulated, and ERA-Interim air temperature and GPH at sounding locations. Figures 5b1, 5b2, 5c1, and 5c2 present biases and RMS errors in each simulation and ERA-Interim reanalysis versus radio soundings. The surface 2 m air temperature and GPH from ERA-Interim are not compared with radio soundings because every radio sounding station is also a CMA station. The GPH at surface represents the terrain height, which is only model input, and there is no need to give in the plots. Besides, the simulated T2 has already been evaluated with CMA station observations. Also, to keep the subfigures uniform, the surface values are not given in this plot. For both air temperature and GPH, all the data sets show quite

**Table 3**
*Similar to Table 2 But for Mean Bias and RMS Error (RMSE) of T2 (°C) and PSFC (hPa)*

| Metrics case | T2 | | PSFC | |
|---|---|---|---|---|
| | Bias | RMSE | Bias | RMSE |
| CTRL | −3.40 | 4.29 | 2.32 | 3.28 |
| CH | −2.79 | 3.95 | 1.69 | 2.76 |
| BBW | −2.41 | 3.83 | 1.60 | 2.61 |
| CHBBW | −2.08 | 3.66 | 1.29 | 2.40 |

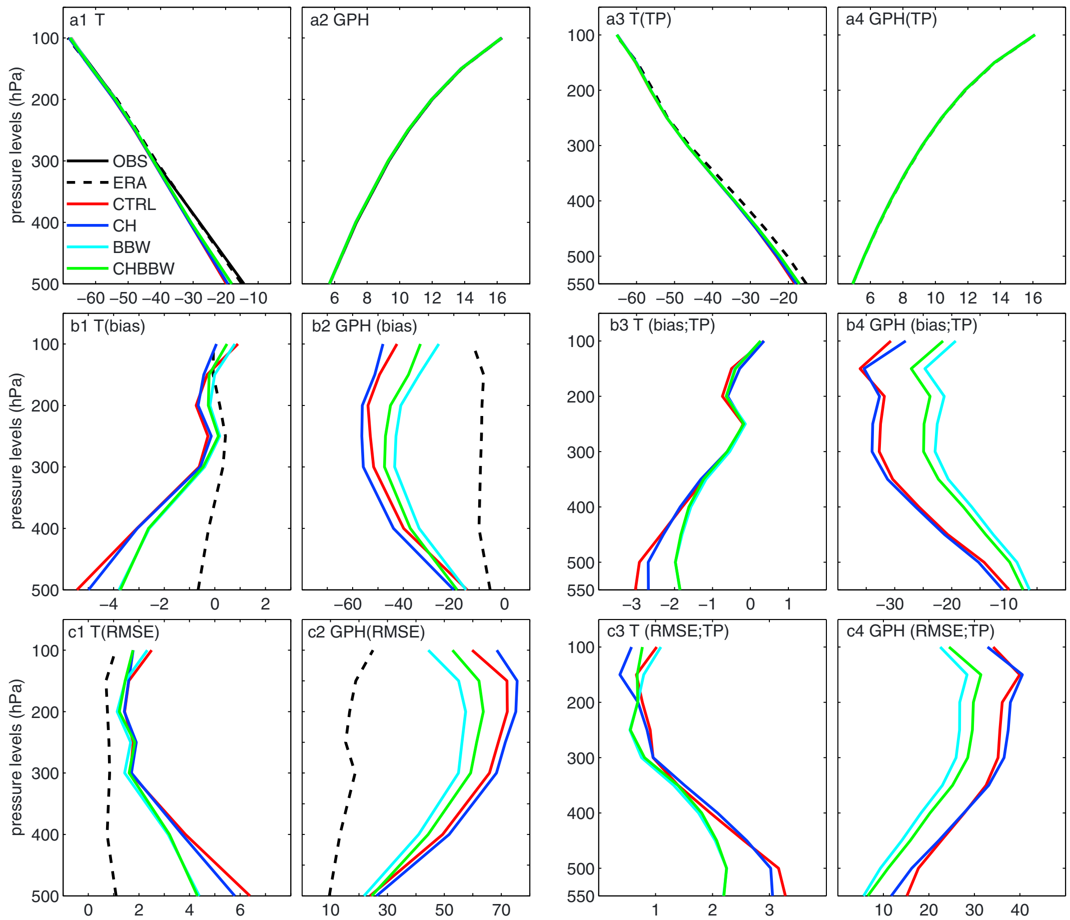

**Figure 5.** Vertical structure of the air temperature (T; °C) and GPH (km) derived from radio soundings, ERA-Interim, and four simulations (a1 and a2 for station mean; a3 and a4 for the whole TP region); and the biases (b1 and b2 for station mean; b3 and b4 for the whole TP region) and RMS errors (c1 and c2 for station mean; c3 and c4 for the whole TP region) of the air temperature and GPH (m) derived from CTRL run, CH run, BBW run, and CHBBW run versus radio sounding data (from daily mean), and versus ERA-Interim (from monthly mean).

similar vertical patterns at radio sounding locations. ERA-Interim has better agreement with observations than the model simulations (characterized by a better vertical pattern, smaller biases, and RMS errors). This is likely to be due to the assimilation of the soundings in ERA-Interim as for the wind components.

When compared with radio soundings, all the runs present a cold bias decrease from 500 hPa to 300 hPa. The BBW and CHBBW runs show better performance with smaller cold biases than the CTRL and CH runs especially at low levels. The improvements of subgrid drag on the GPH are more obvious at the upper levels with the better performance of BBW and CHBBW runs compared to the CTRL and CH runs. The results reveal the uplifting effect by the low-level warmer air in the BBW and CHBBW runs compared to the CTRL and CH runs. The RMS errors generally confirm the vertical pattern of biases in the air temperature and GPH.

When compared with ERA-Interim for the TP regional average, all the data sets also show quite similar vertical patterns. The biases and RMS errors generally follow the patterns seen from the radio soundings. Nevertheless, this comparison gives us a quantitative impression of the model's performance for the whole TP region.

## 5. Discussion

The changes in surface wind in the CH, BBW, and CHBBW runs, when compared with the CTRL run, are the direct results of the subgrid drag added in these simulations. The total subgrid orographic stress from the CH run (GF stress only), the BBW run (TOFD stress only), and the CHBBW run (both GF stress and TOFD stress) are given in Figures 6a–6c respectively, and the partitioning of GF and TOFD stresses in the CHBBW run is

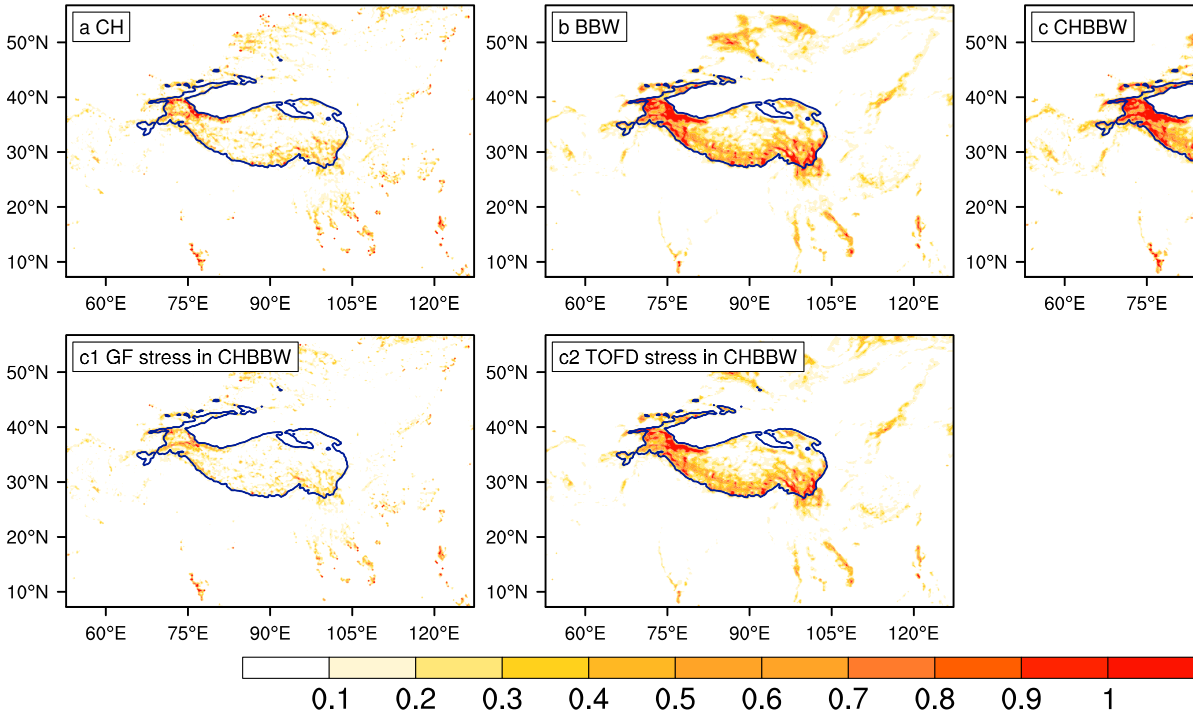


**Figure 6.** Surface stresses due to subgrid orography (N/m$^2$) in (a) CH run, (b) BBW run, and (c) CHBBW run; and the (c1) GF drag and (c2) TOFD drag in CHBBW run.

given separately in Figures 6c1–6c2. Stronger stress corresponds to a larger impact on the total wind speed as discussed. Both the GF stress and TOFD stress in the CHBBW run (where TOFD stress plays a dominant role) show a smaller magnitude compared with those from the individual simulation in the CH and BBW runs, but the total stress in CHBBW is larger than in CH or BBW. The reason is that orographic stress is typically proportional to the square of wind speed, and the impact is to slow down the wind. Theoretically, if one scheme reduces wind speed, the other scheme will become less active. The impact on the surface 10 m wind fields by the GWD/FB scheme is strong (as shown in CH run in Figure 2), but rather weak stress is present when integrated for all the atmosphere layers. The reason is clear from the TP-averaged *u*

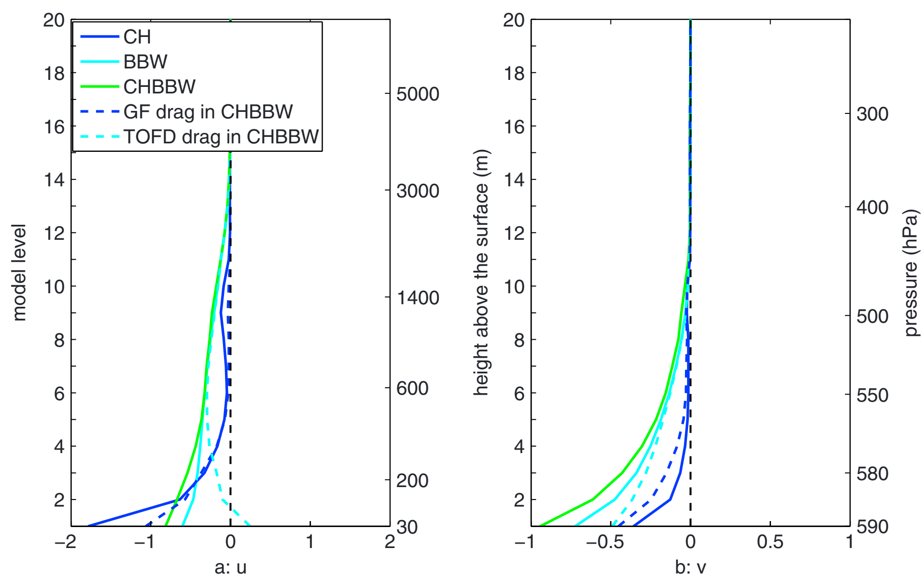


**Figure 7.** The contribution of each subgrid orographic drag to the mean wind tendencies (10$^{-3}$ m/s$^2$; (a) *u* component; (b) *v* component) from first model level (about 30 m above the terrain) to 20th model level (about 11 km height) in CH run, BBW run, and CHBBW run.

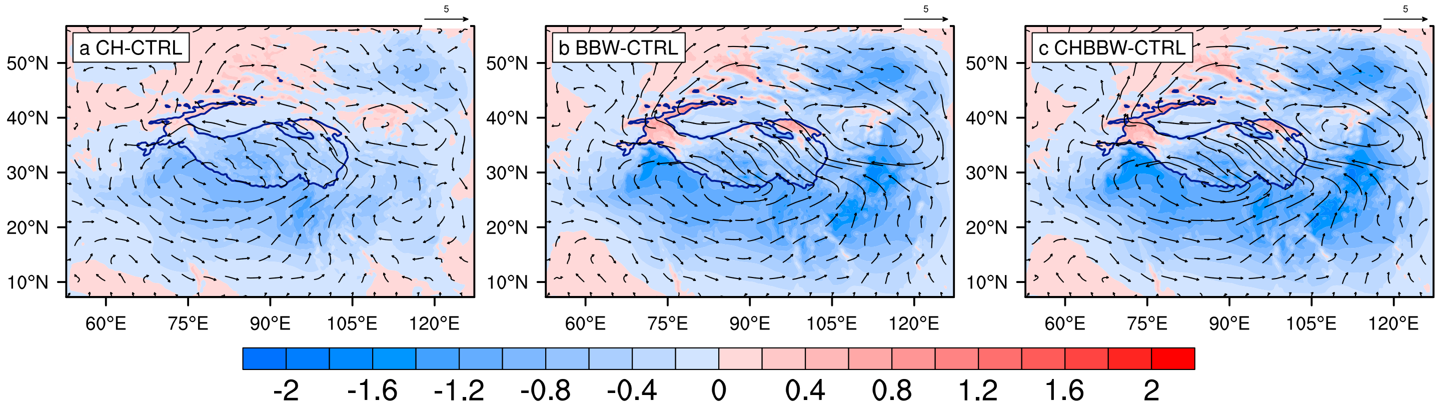


**Figure 8.** Differences of mean change in PSFC (color; hPa) and 500 hPa wind speed (vector) derived from (a) CH run, (b) BBW run, and (c) CHBBW run minus CTRL run.

tendency profiles in Figure 7: The lowest model level *u* tendency in the CH run is larger than in the other runs, but above that the tendency is smaller. In other words, the GF drag (CH run) is limited to the shallow surface layer whereas TOFD in the BBW run is spread over a deep layer. GF is virtually zero above level 6 (about 550 hPa), whereas TOFD shows tendencies up to level 13 (about 400 hPa). It is also worth noting that the lowest layer has a thickness of 60 m only so its contribution to the vertical integral is small. The particular strong GF drag in the lowest model layer also explains its large impact on u10 in the CH and CHBBW runs when evaluating with station data, while the BBW scheme shows moderate impact (Table 2). The interpretation of *v* tendencies is more complex, particularly because the *v* wind is much weaker, has a complex vertical structure, and the wind profile changes as a response to the subgrid orography schemes (see also Figures 3a2 and 3a4). On one hand, the surface orographic stress directly leads to momentum loss and decrease the low-level wind speed; on the other hand, it induces nonlinear impacts on the upper atmosphere and nonmountainous regions through atmosphere circulation.

The enhancement of subgrid orographic drag leads to a change in surface pressure (Figure 8) and air temperature (Figure 9) through their dynamical impacts on the large-scale circulation (Figure 8) and local impact on the land-atmosphere interaction (could be associated with the wind speed modulation of turbulent heat fluxes). In the current study, only the dynamical impacts are highlighted, and more detailed investigations are required to study the impact of the subgrid orographic drag on local land-atmosphere interaction in further work. The lower pressure in the sensitivity runs is more prominent over the southern areas of the domain, where the subgrid orography variability is most pronounced (Figure 1). As suggested by Zadra et al. (2003), the widespread lower pressure in these runs can be interpreted as the result of a new geostrophic balance in the CH, BBW, and CHBBW runs. The higher T2 in these runs are more obvious over East Asia and can be explained by the changed atmosphere circulation and the associated wind field (Figure 8). Dynamically, the changed wind field obviously leads to less cold air transport from the northwestern area to East Asia. Our finding, that the enhancement of the total drag over TP and surroundings leads to lower pressure over

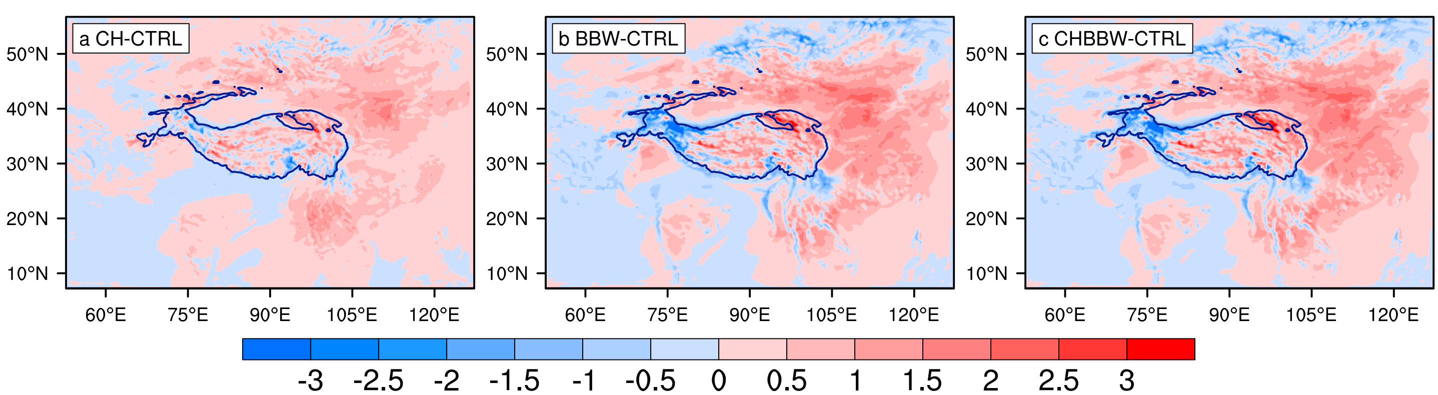


**Figure 9.** Differences of mean change in T2 (°C) derived from (a) CH run, (b) BBW run, and (c) CHBBW run minus CTRL run.

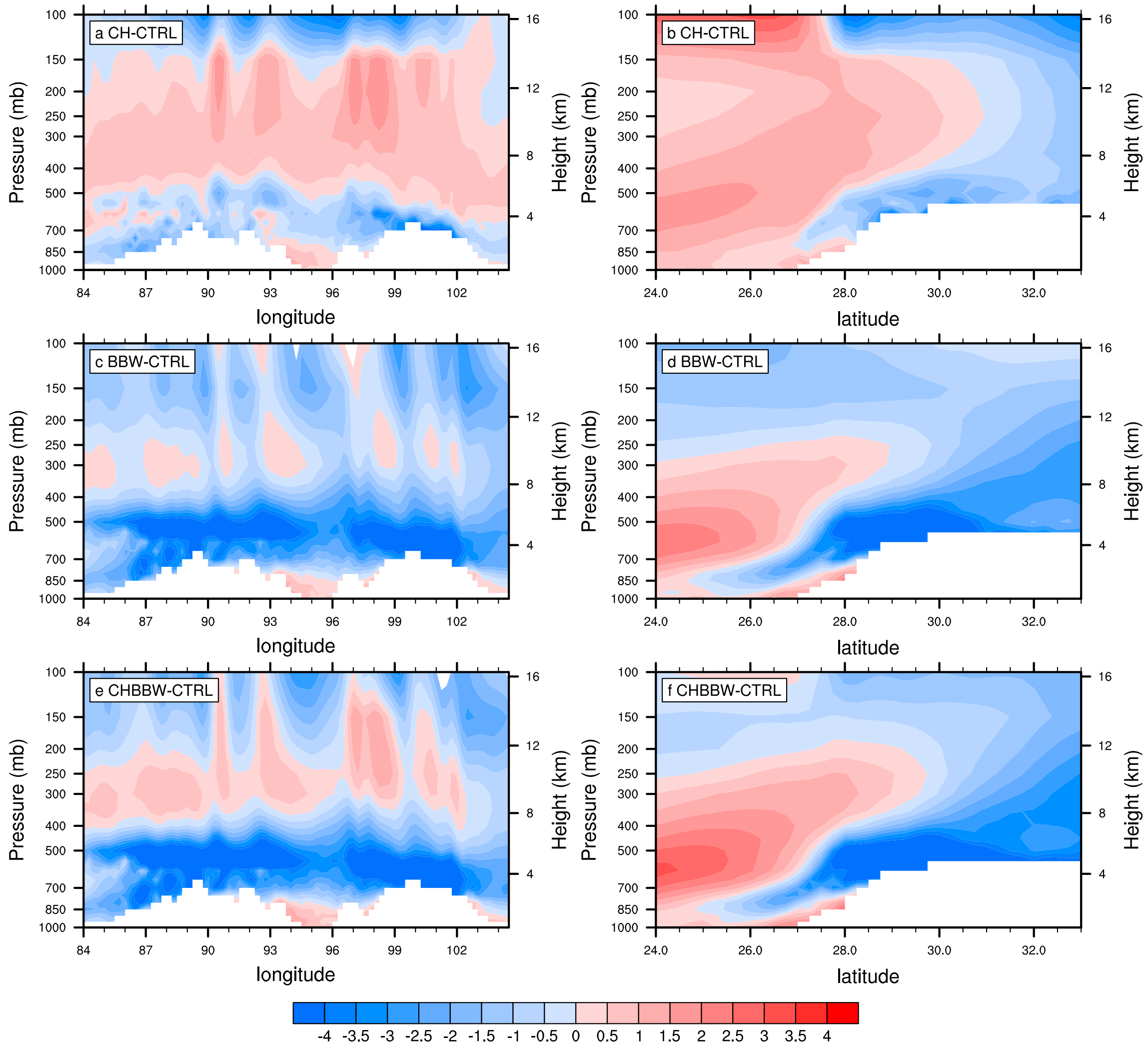


**Figure 10.** Differences of zonal wind (m/s) along (a, c, and e) a zonal cross section averaged over 27°N–30°N, and along (b, d, and f) a meridional cross section averaged over 88°E–94°E derived from CH run, BBW run, and CHBBW run minus CTRL run.

South Asia and East Asia (including most southern part of TP), is in agreement with the subgrid orographic drag enhancement experiment by Sandu et al. (2016).

Focusing on the TP southern boundary, where the Himalaya Mountain range is located, the changes in the $u$ and $v$ profiles in the CH, BBW, and CHBBW runs are given in Figures 10 and 11, respectively. This region is dominated by widespread westerlies; thus, the enhanced subgrid orographic stress induces a new geostrophic balance characterized by weakened low-level zonal wind (Figure 10) and a stronger a-geostrophic wind component. The latter implies a more northward wind at low levels; that is, stronger flow where $v$ is already positive and weaker flow where $v$ is negative (Figure 11). As a result, more warm air is transported across the Himalaya Mountain range to the interior TP from South Asia or less cold air is transported from the north.

## 6. Summary and Further Work

Four sets of experiments have been conducted with different selections of subgrid drag (CTRL run, CH run, BBW run, and CHBBW run, respectively) in a winter month with negligible precipitation (December 2007). The simulation results have been evaluated with CMA station measurements, radio soundings, and ERA-Interim reanalysis data.

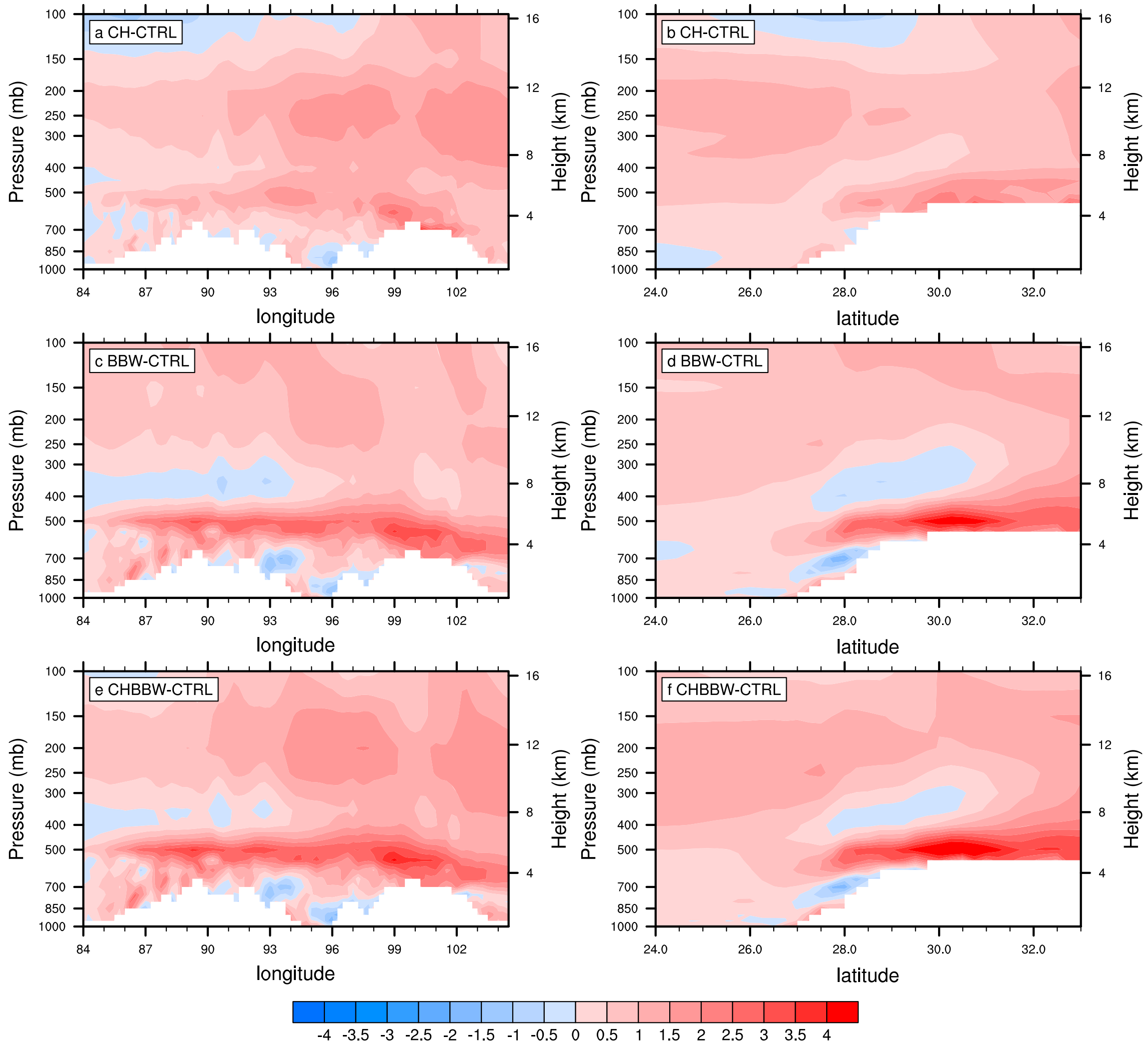


**Figure 11.** Differences of meridional wind (m/s) along (a, c, and e) a zonal cross section averaged over 27°N–30°N, and along (b, d, and f) a meridional cross section averaged over 88°E–94°E derived from CH run, BBW run, and CHBBW run minus CTRL run.

With the different selections of subgrid orographic drag in WRF over the TP, the above simulations reveal that (1) the GWD/FB scheme from Choi and Hong (2015) efficiently reduces the U10 mean bias and RMS error. (2) The TOFD scheme from Beljaars et al. (2004) is more effective in reducing the U10 bias and RMS error. (3) The combination of these schemes in the CHBBW run has the best performance, with smallest station mean bias (−0.18 m/s) and RMS error (0.79 m/s) in simulated U10. (4) Consistent improvements are seen in T2 and PSFC where the CHBBW run shows the best performance, characterized by its smallest station mean bias (−2.05°C for T2 and 1.27 hPa in PSFC) and RMS error (3.59°C in T2 and 2.37 hPa in PSFC). (5) For the vertical distribution of wind components, air temperature and GPH, the BBW TOFD scheme is the main contributor to the improvements (both BBW and CHBBW are better than CTRL and CH).

Our results highlight the importance of the subgrid orographic drag parameterizations in WRF in the simulation of the atmosphere circulation over the TP region. The TP region is dominated by widespread westerlies in winter and enhanced low-level drag directly decelerates the zonal wind and modulates the meridional wind more northward (drag induces a-geostrophic flow resulting in a new geostrophic balance). As a result, the meridional PSFC and T2 gradients are improved in the sensitivity runs with stronger drag over TP and surroundings when compared with the CTRL run.

In summary, the TOFD drag mainly contributes to the improvements in simulating an accurate atmospheric circulation for our model domain. The GF drag also shows effective contributions, though it may cause too strong drag at the surface. With the above evaluations and discussions, we suggest that TOFD scheme from Beljaars et al. (2004) implemented by Zhou et al. (2017) should be switched on in the WRF model to simulate a more realistic atmospheric circulation (especially for regional simulations over the TP in winter). The GWD/FB scheme implemented by Choi and Hong (2015) might be optional, and one may expect more benefits for large-scale simulations, for example, a global run.

In current study, only the YSU PBL scheme is used. However, the orographic drag is related to the turbulence intensity (Xu & Taylor, 1995) which is modulated by the PBL scheme selected in the simulation. Thus, further work could include testing these subgrid drag schemes using the other PBL schemes. Meanwhile, our study only shows regional results over TP in a winter from a monthly mean aspect. And the work should be complemented by more detailed studies. For example, the impacts of these subgrid drag over other regions, other seasons, and the details of the diurnal effects of these subgrid drag schemes (e.g., impacts on the surface energy balance associated turbulent fluxes in land-atmosphere interactions).

**Acknowledgments**

There is no conflict of interests for any author. Other affiliations for any author that may be perceived as having a conflict of interest with respect to the results of this paper. The simulations were performed at the HPCC super computer working station at Institute of Tibetan Plateau Research. For data access, please contact xuzhou@itpcas.ac.cn. Observational data used in this study are available at the given webpage or cited references given in the text and also available by contacting xuzhou@itpcas.ac.cn. The ERA-Interim reanalysis data can be downloaded from https://www.ecmwf.int/en/forecasts/datasets. This work was jointly funded by the Ministry of Science and Technology of the People's Republic of China (grant 2015CB953703 and 2013CBA01800) and by the National Natural Science Foundation of China (grant 91537210, 41325019, and 41705084).

## References

Bao, X. H., & Zhang, F. Q. (2013). Evaluation of NCEP-CFSR, NCEP-NCAR, ERA-Interim, and ERA-40 reanalysis datasets against independent sounding observations over the Tibetan Plateau. *Journal of Climate*, *26*(1), 206–214. https://doi.org/10.1175/Jcli-D-12-00056.1

Beljaars, A. C. M., Brown, A. R., & Wood, N. (2004). A new parametrization of turbulent orographic form drag. *Quarterly Journal of the Royal Meteorological Society*, *130*(599), 1327–1347. https://doi.org/10.1256/qj.03.073

Boer, G. J., McFarlane, N. A., Laprise, R., Henderson, J. D., & Blanchet, J. P. (1984). The Canadian Climate Centre spectral atmospheric general circulation model. *Atmosphere-Ocean*, *22*(4), 397–429. https://doi.org/10.1080/07055900.1984.9649208

Chen, F., & Dudhia, J. (2001). Coupling an advanced land surface-hydrology model with the Penn State-NCAR MM5 modeling system. Part II: Preliminary model validation. *Monthly Weather Review*, *129*(4), 587–604. https://doi.org/10.1175/1520-0493(2001)129<0587:Caalsh>2.0.Co;2

Choi, H. J., & Hong, S. Y. (2015). An updated subgrid orographic parameterization for global atmospheric forecast models. *Journal of Geophysical Research: Atmospheres*, *120*, 12,445–12,457. https://doi.org/10.1002/2015JD024230

Dee, D. P., Uppala, S. M., Simmons, A. J., Berrisford, P., Poli, P., Kobayashi, S., … Vitart, F. (2011). The ERA-Interim reanalysis: Configuration and performance of the data assimilation system. *Quarterly Journal of the Royal Meteorological Society*, *137*(656), 553–597. https://doi.org/10.1002/qj.828

Grant, A. L. M., & Mason, P. J. (1990). Observations of boundary-layer structure over complex terrain. *Quarterly Journal of the Royal Meteorological Society*, *116*(491), 159–186.

Gregory, D., Shutts, G. J., & Mitchell, J. R. (1998). A new gravity-wave-drag scheme incorporating anisotropic orography and low-level wave breaking: Impact upon the climate of the UK Meteorological Office Unified Model. *Quarterly Journal of the Royal Meteorological Society*, *124*(546), 463–493. https://doi.org/10.1256/smsqj.54605

Hong, S. Y., Choi, J., Chang, E. C., Park, H., & Kim, Y. J. (2008). Lower-tropospheric enhancement of gravity wave drag in a global spectral atmospheric forecast model. *Weather and Forecasting*, *23*(3), 523–531. https://doi.org/10.1175/2007waf2007030.1

Hong, S. Y., Noh, Y., & Dudhia, J. (2006). A new vertical diffusion package with an explicit treatment of entrainment processes. *Monthly Weather Review*, *134*(9), 2318–2341. https://doi.org/10.1175/Mwr3199.1

Jimenez, P. A., & Dudhia, J. (2012). Improving the representation of resolved and unresolved topographic effects on surface wind in the WRF model. *Journal of Applied Meteorology and Climatology*, *51*(2), 300–316. https://doi.org/10.1175/Jamc-D-11-084.1

Kim, Y. J. (1996). Representation of subgrid-scale orographic effects in a general circulation model: 1. Impact on the dynamics of simulated January climate. *Journal of Climate*, *9*(11), 2698–2717. https://doi.org/10.1175/1520-0442(1996)009<2698:Rossoe>2.0.Co;2

Kim, Y. J., & Arakawa, A. (1995). Improvement of orographic gravity-wave parameterization using a mesoscale gravity-wave model. *Journal of the Atmospheric Sciences*, *52*, 1875–1902.

Kim, Y. J., & Doyle, J. D. (2005). Extension of an orographic-drag parametrization scheme to incorporate orographic anisotropy and flow blocking. *Quarterly Journal of the Royal Meteorological Society*, *131*(609), 1893–1921. https://doi.org/10.1256/qj.04.160

Lorente-Plazas, R., Jimenez, P. A., Dudhia, J., & Montavez, J. P. (2016). Evaluating and improving the impact of the atmospheric stability and orography on surface winds in the WRF model. *Monthly Weather Review*, *144*(7), 2685–2693. https://doi.org/10.1175/Mwr-D-15-0449.1

Lott, F., & Miller, M. J. (1997). A new subgrid-scale orographic drag parameterization: Its formulation and testing. *Quarterly Journal of the Royal Meteorological Society*, *123*, 101–127. https://doi.org/10.1002/qj.49712353704

Mcfarlane, N. A. (1987). The effect of orographically excited gravity-wave drag on the general-circulation of the lower stratosphere and troposphere. *Journal of the Atmospheric Sciences*, *44*(14), 1775–1800. https://doi.org/10.1175/1520-0469(1987)044<1775:Teooeg>2.0.Co;2

Mlawer, E. J., Taubman, S. J., Brown, P. D., Iacono, M. J., & Clough, S. A. (1997). Radiative transfer for inhomogeneous atmospheres: RRTM, a validated correlated-k model for the longwave. *Journal of Geophysical Research: Atmospheres*, *102*, 16,663–16,682. https://doi.org/10.1029/97JD00237

Palmer, T. N., Shutts, G. J., & Swinbank, R. (1986). Alleviation of a systematic westerly bias in general-circulation and numerical weather prediction models through an orographic gravity-wave drag parametrization. *Quarterly Journal of the Royal Meteorological Society*, *112*(474), 1001–1039. https://doi.org/10.1002/qj.49711247406

Rontu, L. (2006). A study on parametrization of orography-related momentum fluxes in a synoptic-scale NWP model. *Tellus A*, *58*(1), 69–81. https://doi.org/10.1111/j.1600-0870.2006.00162.x

Sandu, I., Bechtold, P., Beljaars, A., Bozzo, A., Pithan, F., Shepherd, T. G., & Zadra, A. (2016). Impacts of parameterized orographic drag on the Northern Hemisphere winter circulation. *Journal of Advances in Modeling Earth Systems*, *8*(1), 196–211. https://doi.org/10.1002/2015ms000564

Scinocca, J. F., & McFarlane, N. A. (2000). The parametrization of drag induced by stratified flow over anisotropic orography. *Quarterly Journal of the Royal Meteorological Society*, *126*(568), 2353–2393. https://doi.org/10.1256/smsqj.56801

Webster, S., Brown, A. R., Cameron, D. R., & Jones, C. P. (2003). Improvements to the representation of orography in the Met Office Unified Model. *Quarterly Journal of the Royal Meteorological Society*, *129*(591), 1989–2010. https://doi.org/10.1256/qj.02.133

Wood, N., Brown, A. R., & Hewer, F. E. (2001). Parametrizing the effects of orography on the boundary layer: An alternative to effective roughness lengths. *Quarterly Journal of the Royal Meteorological Society*, *127*(573), 759–777. https://doi.org/10.1256/smsqj.57302

Wood, N., & Mason, P. (1993). The pressure force induced by neutral, turbulent-flow over hills. *Quarterly Journal of the Royal Meteorological Society*, *119*(514), 1233–1267. https://doi.org/10.1002/qj.49711951402

Wu, G. X., & Chen, S. J. (1985). The effect of mechanical forcing on the formation of a mesoscale vortex. *Quarterly Journal of the Royal Meteorological Society*, *111*(470), 1049–1070. https://doi.org/10.1256/smsqj.47008

Xu, D. P., & Taylor, P. A. (1995). A note on the constants used in $E$-$\epsilon$-$\tau$ turbulence closure. *Boundary-Layer Meteorology*, *72*(1–2), 205–211. https://doi.org/10.1007/Bf00712395

Zadra, A. (2013). *WGNE Drag Project: An Inter-Model Comparison of Surface Stresses*. http://collaboration.cmc.ec.gc.ca/science/rpn/drag_project/documents/wgne_drag_project_report01.pdf

Zadra, A., Roch, M., Laroche, S., & Charron, M. (2003). The subgrid-scale orographic blocking parametrization of the GEM model. *Atmosphere-Ocean*, *41*(2), 155–170. https://doi.org/10.3137/ao.410204

Zhou, X., Yang, K., & Wang, Y. (2017). Implementation of a turbulent orographic form drag scheme in WRF and its application to the Tibetan Plateau. *Climate Dynamics*, 1–13. https://doi.org/10.1007/s00382-017-3677-y